Topology change in commuting saddles of thermal $\mathcal{N} = 4$ SYM theory

Umut Gürsoy

CPHT, École Polytechnique, UMR du CNRS 7644,
91128 Palaiseau, France, and
LPT, École Normale Supérieure,
75231 Paris 05, France
E-mail: gursoy@cpht.polytechnique.fr

Sean A. Hartnoll

KITP, University of California Santa Barbara,
CA 93106, U.S.A.
E-mail: hartnoll@kitp.ucsb.edu

Timothy J. Hollowood and S. Prem Kumar

Department of Physics, University of Wales Swansea,
Swansea, SA2 8PP, U.K.
E-mail: s.p.kumar@swansea.ac.uk, t.hollowood@swansea.ac.uk

ABSTRACT: We study the large N saddle points of weakly coupled $\mathcal{N} = 4$ super Yang-Mills theory on $\boldsymbol{S}^1 \times \boldsymbol{S}^3$ that are described by a commuting matrix model for the seven scalar fields $\{A_0, \Phi_J\}$. We show that at temperatures below the Hagedorn/'deconfinement' transition the joint eigenvalue distribution is $\boldsymbol{S}^1 \times \boldsymbol{S}^5$. At high temperatures $T \gg 1/R_{\boldsymbol{S}^3}$, the eigenvalues form an ellipsoid with topology $\boldsymbol{S}^6$. We show how the deconfinement transition realises the topology change $\boldsymbol{S}^1 \times \boldsymbol{S}^5 \to \boldsymbol{S}^6$. Furthermore, we find compelling evidence that when the temperature is increased to $T = 1/(\sqrt{\lambda} R_{\boldsymbol{S}^3})$ the saddle with $\boldsymbol{S}^6$ topology changes continuously to one with $\boldsymbol{S}^5$ topology in a new second order quantum phase transition occurring in these saddles.

KEYWORDS: 1/N Expansion, AdS-CFT Correspondence, Black Holes in String Theory, Thermal Field Theory.

JHEP11(2007)020

Contents

1. Introduction and summary

In this work we will combine two strands of research that have each generated interesting results within the AdS/CFT correspondence [1] over the past couple of years.

On the one hand, it has been understood how the dynamics of certain supersymmetric sectors of $\mathcal{N} = 4$ super Yang-Mills theory on a spatial S^3 are described by matrix models for the scalar fields Φ_J of the theory. Furthermore, it was discovered that the eigenvalue distributions of these scalars directly reconstruct a dual spacetime geometry [2–5]. These

works have provided a striking realisation of emergent geometry within the AdS/CFT setup.

On the other hand, in the same theory at finite temperature it was shown that at weak 't Hooft coupling there is a phase transition at a critical temperature [6, 7]. This transition appears to be similar to the Hawking-Page transition at strong coupling, which describes the appearance of a black hole in the dual geometry [8, 9]. In particular, for both phase transitions the eigenvalue distribution of the time component of the gauge field, A_0, becomes a nonuniform distribution on $\boldsymbol{S}^1$ at the transition and ultimately becomes a gapped distribution as the temperature is increased.

Combining the insights of these works, one might hope that studying the joint eigenvalue distribution of $\{A_0, \Phi_J\}$ could lead to an understanding of the dual black hole geometry in the weak coupling regime. In fact, a fundamental question is whether or not there is a well defined sense in which it is useful to conceive of a weakly coupled plasma as being dual to a black hole. Various recent works have posed this as a question about correlators in real time physics [10 − 14]. The question is not purely of conceptual interest, as some discussion of the fireball created in the Relativistic Heavy Ion Collider attests, see for instance [15, 16]. The approach here will be Euclidean and hence concerned with equilibrium physics.

In most works on the finite temperature theory at weak coupling, the scalar fields are integrated out on the grounds that they acquire thermal masses, as well as having a classical mass due to being conformally coupled to a spatial $\boldsymbol{S}^3$. However, at temperatures $TR \sim \lambda^{-1/2}$, the one loop thermal mass of A_0 is of the same magnitude as that for the scalar fields, so A_0 and Φ_J (and indeed the A_i [17]) should participate equally in the dynamics. The full dynamics of the theory is difficult to study, as there are infinitely many coupled modes that can condense, and furthermore generic condensates will not commute. In this work we will make the drastic (but consistent) simplification of only considering saddles in which the homogeneous modes of $\{A_0, \Phi_J\}$ condense and where the condensates commute. We believe that these are interesting saddles to consider; they are the most 'geometric' of possible saddles at weak coupling and can be described very explicitly. They may also have a connection with the dominant geometrical saddles at strong coupling. At low temperatures, we may expect such a geometric connection in the spirit of the work of [4]. However, it is clear [17] at high temperatures, that they are not the absolute minima of the theory. Phase transitions in these saddles are not transitions of the full theory.

The effective potential necessary for this study, the potential for commuting scalars and A_0, was computed in [18], who used it to show that the potential reveals a weak coupling analogue of the Gregory-Laflamme instability of the small black hole towards localisation on $\boldsymbol{S}^5$ [18]. In [19] it was found that allowing one scalar field to be non-zero leads to a non-trivial joint eigenvalue distribution of $\{A_0, \Phi_J\}$. This is due to a logarithmic repulsion between the scalar eigenvalues at large N overcoming the classical and thermal mass terms. However, the solutions found in [19] break R symmetry in picking out a given scalar field.

In this work we find the eigenvalue distribution of $\{A_0, \Phi_J\}$ that minimises the one loop effective potential of $\mathcal{N} = 4$ super Yang-Mills theory on $\boldsymbol{S}^1 \times \boldsymbol{S}^3$, when restricted to commuting matrices for the homogeneous modes of A_0 and Φ_J. Our results cover the whole

range of temperatures and couplings for which the one loop potential is valid: $TR \ll \lambda^{-1}$. We use R to denote the radius of the spatial $\boldsymbol{S}^3$. As well as finding the minimal action distribution, which preserves SO(6) R symmetry, in appendix B we exhibit other interesting saddle points of the effective action with various patterns of R symmetry breaking.

In the supersymmetric sector, the logarithmic repulsion between — and subsequent condensation of — scalar eigenvalues is crucial for the emergence of a dual spacetime geometry in the large N limit [4, 5]. This effect needs to be considered also at finite temperature. A central result of our work is that at high temperatures $TR = \lambda^{-1/2}$, the condensate of scalar eigenvalues backreacts sufficiently onto the distribution of the A_0 eigenvalues to cause a new phase transition, in the commuting matrix saddle.

1.1 Summary of results on the eigenvalue distribution

At low temperatures we find analytically that the eigenvalues are uniformly distributed as $\boldsymbol{S}^1 \times \boldsymbol{S}^5$. Here the $\boldsymbol{S}^1$ is in the A_0 direction whereas the $\boldsymbol{S}^5$ is in the Φ_J directions and has a radius that scales like λ/R.

At the deconfinement temperature, $TR_c = -1/\log(7-4\sqrt{3}) \approx 0.38$ [7], the distribution on $\boldsymbol{S}^1$ develops a gap. We show analytically that this implies that the full distribution acquires topology $\boldsymbol{S}^6$.

At high temperatures, $1 \ll TR \ll \lambda^{-1}$, we find two candidate saddle points. There is an $\boldsymbol{S}^5$ distribution that can be described analytically and an ellipsoidal distribution with topology $\boldsymbol{S}^6$ that we obtain analytically for $TR \ll \lambda^{-1/2}$ and numerically at higher temperatures. The $\boldsymbol{S}^5$ solution is at a point in the A_0 direction. Both solutions preserve the full SO(6)$_R$ symmetry.

At weak coupling, we find that the ellipsoidal solution has lowest action at temperatures $TR_c \leq TR < \lambda^{-1/2}$. The first result of this paper is therefore that, in the sector of commuting spatially homogeneous fields, the low and high temperature phases of weakly coupled $\mathcal{N} = 4$ SYM theory on $\boldsymbol{S}^3$ are characterised by eigenvalue distributions with differing topology: $\boldsymbol{S}^1 \times \boldsymbol{S}^5$ versus $\boldsymbol{S}^6$. As the temperature is increased to the value $TR = \lambda^{-1/2}$ at fixed weak coupling, or equivalently, as the coupling is increased up to $\lambda = 1/(TR)^2$ at fixed high temperatures, we find compelling evidence for a second order phase transition. In this transition the $\boldsymbol{S}^6$ solution smoothly collapses to $\boldsymbol{S}^5$. We summarize the behaviour of these saddles in figure 1 below. Details will be discussed below.

2. The effective potential

Our starting point is the one loop effective potential of $\mathcal{N} = 4$ SYM theory on $\boldsymbol{S}^1 \times \boldsymbol{S}^3$, restricted to a certain sector of the theory. We denote the radius of the $\boldsymbol{S}^3$ by R and $\beta = 1/T$ will be the circumference of the thermal $\boldsymbol{S}^1$. The effective potential is the result of integrating out all inhomogeneous modes on the three sphere and depends only on the homogeneous modes. The latter are the vacuum expectation values of the six scalar fields in the theory, Φ_J, $J = 1, 2, \ldots, 6$,[1] and the time component of the gauge field, A_0. This potential was computed in [18] and also discussed recently in [19].

---

[1] We denote a six vector with a boldface symbol, e.g. $\boldsymbol{\Phi}$ and $\boldsymbol{\phi}$.
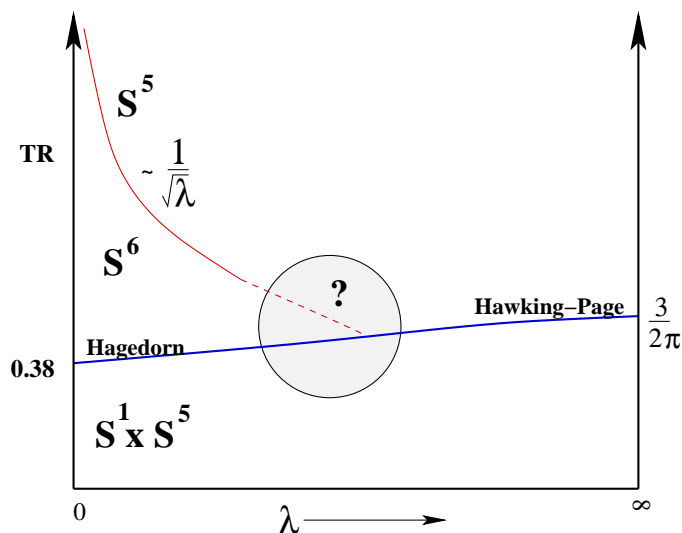
Figure 1: Topology of the dominant eigenvalue distribution in which the only the homogeneous modes of $\{A_0, \Phi_J\}$ condense and furthermore commute.

An important feature of the effective potential is that it is evaluated on the space of mutually commuting scalar homogeneous modes. The potential is therefore a function of the eigenvalues of the adjoint scalars, which we denote by $\{\phi_p\}$, $p = 1, 2, \ldots, N$, and the eigenvalues of βA_0, which we denote by $\{\theta_p\}$.

It is natural to consider the effective potential on the space of commuting scalar field expectation values. In flat space and at zero temperature, these characterize the moduli space of vacua of the $\mathcal{N} = 4$ theory, wherein off diagonal modes obtain masses $|\phi_{pq}|$.[2] There is no moduli space on $\boldsymbol{S}^3$ due to the classical conformal coupling to the background scalar curvature. However, around a homogeneous background with commuting VEVs for the scalars, off diagonal fluctuations of the scalar zero modes obtain a positive mass given by $\sqrt{R^{-2} + |\phi_{pq}|^2}$ and those of A_0 have masses $|\phi_{pq}|$. For this reason all the configurations that we consider will be locally stable against small fluctuations involving the off-diagonal entries of the scalar field matrices. This is also manifest in the reality of the one loop effective potential below, on the space of simultaneously diagonal configurations.

We should emphasize that whereas the truncation to commuting matrices is consistent, it will not describe the absolute minimum of the action [17]. We will see however, that these commuting saddles display some interesting dynamics. Throughout this work, we are only considering saddles in which the matrices commute.

A second consistent truncation we have made is to consider condensates for only the homogeneous modes. At infinite N, the inhomogeneous modes can also condense without breaking the spatial SO(4) rotational invariance. The full dynamics should include these modes also.

There are three contributions to the potential: the classical conformal mass term for

---

[2]We set $|\phi| \equiv \sqrt{\sum_J \phi_J^2}$ and $\phi_{pq} = \phi_p - \phi_q$.

the scalars and then two determinants arising from integrating out the bosons and fermions in the theory

$$S_{\text{eff}}[\phi_p, \theta_p] \;=\; S^{(0)} + S_{\text{b}}^{(1)} + S_{\text{f}}^{(1)}\,. \tag{2.1}$$

The classical term is

$$S^{(0)} = \frac{\beta R \pi^2 N}{\lambda} \sum_{p=1}^{N} |\phi_p|^2\,. \tag{2.2}$$

Integrating out the gauge fields, scalar and ghost fluctuations yields the bosonic contribution

$$
\begin{aligned}
S_{\text{b}}^{(1)} = \sum_{pq=1}^{N} \bigg\{ &-\log \left| \sinh \frac{\beta|\phi_{pq}| + i\theta_{pq}}{2} \right| - \log 2 \\
&+ \sum_{\ell=0}^{\infty} 2(2\ell+3)(2\ell+1)\bigg(\frac{\beta}{2}\sqrt{(\ell+1)^2 R^{-2} + |\phi_{pq}|^2} \\
&+ \log \left| 1 - e^{-\beta\sqrt{(\ell+1)^2 R^{-2}+|\phi_{pq}|^2}+i\theta_{pq}} \right| \bigg) \bigg\}\,.
\end{aligned}
\tag{2.3}
$$

Here

$$|\phi_{pq}| = \sqrt{(\phi_p - \phi_q)^2}; \qquad \theta_{pq} = \theta_p - \theta_q. \tag{2.4}$$

The fermion fluctuation determinants contribute

$$
\begin{aligned}
S_{\text{f}}^{(1)} = -\sum_{pq=1}^{N}\sum_{\ell=1}^{\infty} 8\ell(\ell+1)\bigg(&\frac{\beta}{2}\sqrt{(\ell+1/2)^2 R^{-2} + |\phi_{pq}|^2} \\
&+ \log \left| 1 + e^{-\beta\sqrt{(\ell+1/2)^2 R^{-2}+|\phi_{pq}|^2}+i\theta_{pq}} \right| \bigg)\,.
\end{aligned}
\tag{2.5}
$$

The validity of the one loop potential requires weak 't Hooft coupling, $\lambda \ll 1$, but also $\lambda \ll 1/(TR)$. This is because at $TR \sim \lambda^{-1}$ the spatial S^3 is the same size as the non-perturbatively generated magnetic screening scale. Our objective is now to minimise this potential and analyse how the ground state depends on the temperature and coupling. The Casimir terms in (2.3) and (2.5)[3] can consistently be ignored, since expanding them in ϕ gives terms of the form $\beta R|\phi|^2(1+\mathcal{O}(R^2\phi^2))$ which, at weak coupling, is always subleading compared with the tree level mass term. It is important, however, that we do not ignore the ϕ_{pq} dependence of the exponential terms because these are enhanced at high temperature $TR \to \infty$, and will play a significant rôle in our analysis in this regime.

3. Low temperature distribution: $S^1 \times S^5$

The action at low $RT \ll 1$ is

$$S_{TR\ll 1} = \frac{N\pi^2 R\beta}{\lambda}\sum_{p=1}^{N}|\phi_p|^2 - \sum_{pq=1}^{N}\log\left|\sinh\frac{\beta|\phi_{pq}|+i\theta_{pq}}{2}\right| - N^2\log 2\,. \tag{3.1}$$

---

[3]These are the first terms in the sum over ℓ, involving square roots.

This expression neglects terms in the action (2.1) that are exponentially suppressed at low temperatures. The logarithmic repulsive force generated between the eigenvalues is a generalised Vandermonde type interaction resulting from integrating out the off-diagonal fluctuations; its origin can be traced to the ghost and gauge fixing terms in the action [18]. At $\lambda = 0$, when the scalars identically vanish, it reduces to the measure factor in the unitary matrix model of [7].

The pairwise eigenvalue repulsion is only countered by an external quadratic attractive potential along the scalar field directions. We should therefore expect the lowest energy state to be localized in the scalar directions and maximally spread out, i.e. uniformly distributed, along the $\boldsymbol{S}^1$. In this case, using the fact that

$$\log \left| \sinh \frac{\beta|\boldsymbol{\phi}| + i\theta}{2} \right| = -\log 2 + \frac{\beta}{2}|\boldsymbol{\phi}| - \sum_{n=1}^{\infty} \frac{1}{n} e^{-n\beta|\boldsymbol{\phi}|} \cos(n\theta) , \tag{3.2}$$

and noticing that the periodic pieces will average to zero for a uniform distribution of θ_ps, we have an effective action

$$S_{TR \ll 1} = \frac{N\pi^2 R\beta}{\lambda} \sum_{p=1}^{N} |\boldsymbol{\phi}_p|^2 - \frac{\beta}{2} \sum_{pq=1}^{N} |\boldsymbol{\phi}_{pq}| . \tag{3.3}$$

In fact we will find in the next section that this action is valid all the way up to the confinement/deconfinement transition. One way to see this is to note that, as we do in the next section, that below the confinement/deconfinfement transition the θ_ps are uniformly distributed around $\boldsymbol{S}^1$. Hence, the averaging over them has the same effect in the action as sending $T \to 0$.

It is convenient to introduce the dimensionless variables

$$\boldsymbol{x}_p = \beta\boldsymbol{\phi}_p . \tag{3.4}$$

At large N we can pass to a continuum limit. The eigenvalues are described by a joint distribution in seven dimensions, which satisfies the normalisation condition

$$\frac{1}{N} \sum_{p=1}^{N} \to \int d^6x d\theta \, \rho(\boldsymbol{x}, \theta) = 1 , \tag{3.5}$$

although in the present case $\rho(\boldsymbol{x}, \theta) = \rho(\boldsymbol{x})$ only. The equation of motion for $\boldsymbol{x}$ is

$$\frac{\pi^2 RT}{\lambda} \boldsymbol{x} = \pi \int_D d^6x' \, \rho(\boldsymbol{x}') \frac{\boldsymbol{x} - \boldsymbol{x}'}{|\boldsymbol{x} - \boldsymbol{x}'|} , \tag{3.6}$$

where the eigenvalue distribution has support in some domain $D \subset \boldsymbol{R}^6$ and $\boldsymbol{x} \in D$.

We can see that (3.6) has a solution for which D is an $\boldsymbol{S}^5$ of radius r, which is easily determined. The density is found to be

$$\rho(\boldsymbol{x}) = \frac{\delta(|\boldsymbol{x}| - r)}{2\pi^4 r^5} , \tag{3.7}$$

where the radius r is

$$r = \frac{\lambda}{\pi^3 RT} \frac{1024}{945} . \tag{3.8}$$

This solution coincides with the zero temperature $\boldsymbol{S}^5$ solution of [4] which is what we should expect in the low temperature limit where thermal effects are negligible. Importantly, the smooth $\boldsymbol{S}^5$ is a consequence of the large N limit. The SO(6) symmetry of the $\mathcal{N} = 4$ theory is left unbroken in this saddle by a global SO(6) rotation on each of the $\boldsymbol{x}_p$ combined with the action of the Weyl group of SU(N) which acts through permutations of the $\boldsymbol{x}_p$.

Let us determine the action associated to this $\boldsymbol{S}^5 \times \boldsymbol{S}^1$ geometry of eigenvalues

$$S_{\boldsymbol{S}^5 \times \boldsymbol{S}^1} = \frac{2N^2\pi^3 TR}{\lambda} \int d^6x \, \rho(\boldsymbol{x}) \, \boldsymbol{x}^2 - 4\pi^2 N^2 \int d^6x \int d^6x' \, \rho(\boldsymbol{x})\rho(\boldsymbol{x}') \, \log|\boldsymbol{x} - \boldsymbol{x}'| . \tag{3.9}$$

To this order in perturbation theory, we find that the action for this configuration is

$$\frac{1}{N^2} S_{\boldsymbol{S}^5 \times \boldsymbol{S}^1} = -\frac{\lambda}{\pi^4} \frac{1024^2}{945^2} \frac{1}{TR} . \tag{3.10}$$

The action is lower than that of both the solution in which the scalars have zero expectation value, and also of the band solution found in [19], in which all $\boldsymbol{x}_p$ acquired non-zero expectation values along the same direction in SO(6) space, thus only preserving an SO(5) subgroup of the global symmetry group. It seems very likely that this maximally symmetric saddle is the absolute minimum of the effective potential at low temperatures, within the sector of the theory we are considering. We prove stability against R symmetry breaking perturbations in appendix A. Furthermore, in appendix B we find various other saddle points with reduced R symmetry and find that they have a higher action.

It is striking that the eigenvalue distribution localises to a hypersurface and does not spread out in all the six noncompact dimensions. In fact, we can exclude six dimensional solutions to the effective equation of motion for the scalars (assuming a uniform distribution on $\boldsymbol{S}^1$), by repeated application of the $\boldsymbol{\nabla}$ operator in six dimensions. In particular, acting on equation (3.6) with the operator $\boldsymbol{\nabla}^2(\boldsymbol{\nabla}\cdot)$, we find $\int d^6x' \, \rho(\boldsymbol{x}')/|\boldsymbol{x} - \boldsymbol{x}'|^3 = 0$ which implies a vanishing density in six dimensions. This then implies that the eigenvalues at large N must be constrained to lie on a hypersurface in six dimensions and this is indeed what we find. An argument along similar lines was shown in [4], implying that eigenvalue distributions arising from similar commuting matrix models were always singular. Localisation to a hypersurface is the simplest way to achieve this.

Note that our analysis is consistent with [7] when $\lambda = 0$: the emergent $\boldsymbol{S}^5$ disappears and only the configuration space of eigenvalues of the Polyakov loop remains. As advocated in [2, 4] the large N vacuum configuration of eigenvalues should be interpreted as the emergence, at weak 't Hooft coupling in our case, of the $\boldsymbol{S}^5$ in the dual $\boldsymbol{AdS}_5 \times \boldsymbol{S}^5$ geometry. The connection to a dual geometry is discussed in more detail below.

4. The deconfinement transition: $\boldsymbol{S}^1 \times \boldsymbol{S}^5 \to \boldsymbol{S}^6$

This section describes the distribution for $TR \ll \lambda^{-1/2}$. In particular, we will be interested in the 'deconfinement' or 'Hagedorn' transition that occurs at $TR_c \approx 0.38$ [7]. We will see

that the eigenvalue distribution undergoes a topology change: $\boldsymbol{S}^1 \times \boldsymbol{S}^5 \to \boldsymbol{S}^6$. We will comment on possible spacetime interpretations of this transition in a later section. The details of the transition are accessible within standard perturbation theory in λ which is valid for all temperatures $TR \ll \lambda^{-1/2}$.

To analyze the vicinity of the phase transition we make use of certain properties of the equilibrium distribution of the scalar fields at weak coupling. At an equilibrium, the tree level attractive potential balances out the pairwise repulsive forces generated at one loop. It is straightforward to see that the one loop contribution to the effective action (2.1) can only compete with the tree level term if $|\boldsymbol{x}| \sim \mathcal{O}(\lambda)$. Hence, in order to be consistent with the perturbative expansion we should expand the one loop contribution in powers of $\boldsymbol{x}$. This has the effect of reorganizing the pertubative expansion. The only caveat is that when the temperature is very high, $TR \gtrsim \lambda^{-1/2}$, a further reorganization occurs which we shall describe in a later section. In this section we shall assume that $TR \ll \lambda^{-1/2}$.

We now define $\boldsymbol{x} = \lambda \tilde{\boldsymbol{x}}$ and expand the action up to $\mathcal{O}(\lambda)$ to obtain

$$S = \lambda^0 S^{(0)}(\theta) + \lambda \left(S^{(1)}(\theta, \tilde{\boldsymbol{x}}) + S_{\text{2-loop}}(\theta) \right) + \mathcal{O}(\lambda^2), \tag{4.1}$$

where

$$S^{(0)}[\theta] = \sum_{pq=1}^{N} \sum_{n=1}^{\infty} \frac{1}{n} \left[1 - z_B(e^{-n/TR}) - (-1)^{n+1} z_F(e^{-n/TR}) \right] \cos(n\theta_{pq}) . \tag{4.2}$$

This is precisely the $\lambda = 0$ effective potential of [7]. The single particle partition functions z_B and z_F will be given below. At the Hagedorn transition, the coefficient of the lowest cosine term becomes negative [7]. The one loop term in the action (4.1), using (3.2), is given by:

$$S^{(1)}[\theta, \tilde{\boldsymbol{x}}] = N\pi^2 TR \sum_{p=1}^{N} |\tilde{\boldsymbol{x}}_p|^2 - \frac{1}{2} \sum_{pq=1}^{N} |\tilde{\boldsymbol{x}}_{pq}| \left[1 + 2 \sum_{n=1}^{\infty} \cos(n\theta_{pq}) \right] . \tag{4.3}$$

It is clear from the form of the expansion (4.1) that to leading order the θ_ps are unaffected by the scalars. In other words the θ_p, and their density in the large N limit, behave to leading order exactly as they did with zero scalar VEVs. The scalar VEVs themselves are then, to leading order, determined by finding the minimum of $S^{(1)}(\theta, \tilde{\boldsymbol{x}})$ with the given values for θ_p. Notice that although this term is of the same order as a two loop contribution, the latter contribution only involves the θ_p, as indicated, and therefore doesn't contribute to the leading $\tilde{\boldsymbol{x}}$ distribution.

The term in square brackets in (4.3) is simply the delta function $\pi\delta(\theta_{pq})$, restricted to even functions. Note that the θ eigenvalue density is indeed an even function [7]. Taking the large N limit and describing the eigenvalues by the joint density $\rho(\theta, \tilde{\boldsymbol{x}})$, as previously, we have

$$\frac{1}{N^2} S^{(1)} = \pi^2 TR \int d\theta \, d^6\tilde{x} \, \rho(\theta, \tilde{\boldsymbol{x}}) |\tilde{\boldsymbol{x}}|^2 - \pi \int d\theta \, d^6\tilde{x} \, d^6\tilde{x}' \, \rho(\theta, \tilde{\boldsymbol{x}}) \rho(\theta, \tilde{\boldsymbol{x}}') |\tilde{\boldsymbol{x}} - \tilde{\boldsymbol{x}}'| . \tag{4.4}$$

We now proceed to minimise this action.

The fact that the reduced density

$$\rho(\theta) = \int d^6\tilde{x}\, \rho(\theta, \tilde{x})\,, \tag{4.5}$$

is determined by the zero scalar VEV problem, together with preserving $SO(6)_R$ symmetry, implies that the joint density is

$$\rho(\theta, \tilde{x}) = \frac{\rho(\theta)\delta(|\tilde{x}| - r(\theta))}{|\tilde{x}|^5\sqrt{1 + (dr/d\theta)^2}\,\mathrm{Vol}\,\boldsymbol{S}^5}\,, \tag{4.6}$$

where the unknown function $r(\theta)$ determines the size of the $\boldsymbol{S}^5$ as it is fibred over the support of $\rho(\theta)$. We recall that that we have already argued that other $SO(6)$ symmetric configurations for which the scalar field spectral density has a smooth six dimensional support are not allowed, as in [4]. From (4.6) we have

$$\frac{1}{N^2}S^{(1)} = \pi^2 RT \int d\theta\, \rho(\theta)r(\theta)^2 - \pi\sqrt{2}C \int d\theta\, \rho(\theta)^2 r(\theta)\,, \tag{4.7}$$

where

$$C = \frac{2048\sqrt{2}}{945\pi}\,. \tag{4.8}$$

Completing the square gives

$$\frac{1}{N^2}S^{(1)} = \pi^2 RT \int d\theta \left[\rho(\theta)\left(r(\theta) - \frac{C}{\sqrt{2}\pi TR}\rho(\theta) \right)^2 - \frac{C^2}{2\pi^2(TR)^2}\rho(\theta)^3 \right]\,. \tag{4.9}$$

The final term only depends on θ and simply contributes to the two loop order distribution of the θ_ps. Therefore it can be ignored for our purposes. However, it will potentially influence higher loop computations for determining the order(s) of possible phase transitions at finite coupling [7]

Hence, for a minimum we have

$$r(\theta) = \frac{C}{\sqrt{2}\pi RT}\rho(\theta)\,. \tag{4.10}$$

This result directly connects the shape of the eigenvalue distribution and the eigenvalue density, and implies that the topology change $\boldsymbol{S}^5 \times \boldsymbol{S}^1 \to \boldsymbol{S}^6$ occurs as T is increased through the phase transition. This is because $\rho(\theta)$ changes from the uniform to a gapped distribution with support $-\theta_0 < \theta < \theta_0$, where $\rho(\pm\theta_0) = 0$ [7]. When $\rho(\theta)$ is uniform, the distribution is $\boldsymbol{S}^1 \times \boldsymbol{S}^5$, as in the previous section. Once $\rho(\theta)$ becomes gapped, then the distribution is an $\boldsymbol{S}^5$ fibred over an interval with the size of the $\boldsymbol{S}^5$ vanishing at the endpoints. This is topologically an $\boldsymbol{S}^6$.

We can now check the consistency of our expansion in $\boldsymbol{x}$ by investigating whether the higher terms in the expansion are finite on the solution (4.10). The potentially dangerous higher terms, coming from expanding $e^{-n|\boldsymbol{x}_{pq}|}\cos(n\theta_{pq})$, have the form

$$\sum_{pq=1}^{N}\sum_{n=1}^{\infty} \frac{\lambda^{m+1}}{n}\big|n\tilde{\boldsymbol{x}}_{pq}\big|^{m+1}\cos(n\theta_{pq}) \tag{4.11}$$

$$\sim \int_0^{\pi} d\xi \sin^4\xi \int_{-\theta_0}^{\theta_0} d\theta\, \partial_\theta^m \left[\rho(\theta)\rho(\theta')(\rho(\theta)^2 + \rho(\theta')^2 - 2\rho(\theta)\rho(\theta')\cos\xi)^{(m+1)/2} \right]_{\theta'=\theta}.$$

Here, we used the fact that

$$\sum_{n=1}^{\infty} n^m \cos(n\theta) = \pi \partial_\theta^m \delta(\theta) \,, \tag{4.12}$$

and integrated by parts. The question is whether the terms (4.11) are finite. The potential problem occurs at the edges of the distribution $\theta = \pm\theta_0$ where there are possible singularities. We know [7], see also the following section, that in the vicinity of the edge $\theta = \theta_0$ the density behaves as $\rho(\theta) \sim \sqrt{\theta_0 - \theta}$. It is not difficult to show that the integrals are completely regular at $\theta = \theta_0$. Hence the analysis is consistent across the transition and into the high temperature phase (assuming $(TR)^2 \ll 1/\lambda$).

In summary, inclusion of the lowest order corrections in λ leads to an interpretation of the Hagedorn/deconfinement transition as a topology changing transition, $\boldsymbol{S}^1 \times \boldsymbol{S}^5 \to \boldsymbol{S}^6$, in eigenvalue space. The possible implications of this geometric transition for the dual spacetime will be discussed below.

5. Intermediate temperatures: $\boldsymbol{S}^6$ ellipsoid

We now determine the joint eigenvalue distribution in the temperature range $1 \ll TR \ll \lambda^{-1/2}$ and provide further evidence for the appearance of the $\boldsymbol{S}^6$ topology above the Hagedorn/deconfinement temperature. In this region, the θ_p have the Wigner semi-circular distribution. To see this we have to analyse $S^{(0)}$ for $TR \gg 1$. First of all, recall that the single particle partition functions in (4.2) are given by [7]

$$z_B(x) = \frac{2x(3 + 6x - x^2)}{(1-x)^3}, \qquad z_F(x) = \frac{16x^{3/2}}{(1-x)^3} \,. \tag{5.1}$$

For $TR \gg 1$ this implies

$$z_B(x) \to 16(TR)^3/n^3 \,, \qquad z_F(x) \to 16(TR)^3/n^3 \,, \tag{5.2}$$

and we expect that the θ_p are small at high temperatures, in which case using $\sum_{n=1}^{\infty}(2n-1)^{-2} = \pi^2/8$, we have in this limit

$$S^{(0)} \to -\sum_{pq=1}^{N} \left(\log|\theta_{pq}| - 2\pi^2(TR)^3 \theta_{pq}^2 \right) = -\sum_{pq=1}^{N} \log|\theta_{pq}| + 4N\pi^2(TR)^3 \sum_{p=1}^{N} \theta_p^2 \,. \tag{5.3}$$

This is the action of the conventional Hermitian matrix model with quadratic potential. The saddle point equation is

$$\sum_{q(\neq p)=1}^{N} \frac{1}{\theta_p - \theta_q} = 4N\pi^2(TR)^3 \theta_p \tag{5.4}$$

In the large N limit we can solve for the density in the usual way, by introducing the resolvent

$$\omega(x) = \frac{1}{N} \sum_{p=1}^{N} \frac{1}{x - \theta_p} \,, \tag{5.5}$$

in terms of which (5.4) becomes

$$\omega(\theta + i\epsilon) + \omega(\theta - i\epsilon) = 8\pi^2 (TR)^3 \theta \,, \tag{5.6}$$

for $-\theta_0 \leq \theta \leq \theta_0$ and ϵ is an infinitesimal which imposes on the left hand side a principal value. It follows from (5.5) that

$$\omega(\theta + i\epsilon) - \omega(\theta - i\epsilon) = -2\pi i \rho(\theta) \,, \tag{5.7}$$

where again $-\theta_0 \leq \theta \leq \theta_0$. It then follows from (5.6) and (5.7) that the resolvent $\omega(x)$ is an analytic function of x which has a square root branch cut between $x = \pm\theta_0$. Since $\omega(x)$ must go to zero for large $|x|$ this determines uniquely

$$\omega(x) = 4\pi^2 (TR)^3 \left(x - \sqrt{x^2 - \theta_0^2} \right) \,. \tag{5.8}$$

By taking the discontinuity across the cut we obtain

$$\rho(\theta) = 4\pi (TR)^3 \sqrt{\theta_0^2 - \theta^2} \,. \tag{5.9}$$

Finally, normalising the density gives

$$\theta_0^2 = \frac{1}{2\pi^2 (TR)^3} \,. \tag{5.10}$$

Using (4.10) we see that in this region of intermediately high temperatures the combined density has support on an ellipsoid with topology $\boldsymbol{S}^6$ given by

$$\frac{\pi^2}{\lambda^2 4 C^2 TR} \boldsymbol{x}^2 + 2\pi^2 (TR)^3 \theta^2 = 1. \tag{5.11}$$

Given that $TR\sqrt{\lambda} \ll 1$, this ellipsoid is very elongated in the θ direction. The eigenvalue density (4.6) is largest at the highly pointed tips at $\boldsymbol{x} = 0$.

6. High temperature distributions: $\boldsymbol{S}^6$ versus $\boldsymbol{S}^5$

This section studies the distribution at high temperatures $1 \ll TR \ll 1/\lambda$, which includes $TR \sim \lambda^{-1/2}$. We will see that in this regime the VEVs of the scalar fields are no longer determined by the θ_p, but rather the full coupled system must be considered. The new phenomenon we will find in this regime therefore could not be seen in previous analysis that neglected these scalar VEVs.

It is worth remarking that for $TR \gtrsim \lambda^{-1/2}$, the $\boldsymbol{S}^3$ size exceeds the electric or Debye scale, and perturbation theory in λ is replaced by a perturbation theory in $\sqrt{\lambda}$ due to infrared effects. Importantly for us, our one loop effective potential remains unaltered by these resummations since the associated momentum integrals at high temperatures happen to be insensitive to IR effects.

The analysis of the previous section, however, will break down at high temperatures where $TR \gtrsim \lambda^{-1/2}$ for a different reason. At these temperatures, the distribution of the $\boldsymbol{x}$

will begin to affect the θs. This is precisely the region when the $\boldsymbol{S}^6$ begins to look spherical in the dimensionless variables $\boldsymbol{x}$ and θ. However it is important to realise that the analysis in this section has an overlap with the analysis of the last section when $1 \ll TR \ll \lambda^{-1/2}$.

To see what goes wrong with the earlier analysis look at the corrections (4.11). These are

$$\sum_{pq=1}^{N} \sum_{n=1}^{\infty} \frac{1}{n} |n\boldsymbol{x}_{pq}|^{m+1} \cos(n\theta_{pq}) = \pi \sum_{pq=1}^{N} |\boldsymbol{x}_{pq}|^{m+1} \partial_\theta^m \delta(\theta_{pq}) . \tag{6.1}$$

We can estimate the behaviour of these terms as a function of λ and TR by using the fact that from (5.11) when $TR \gg 1$ we have $\boldsymbol{x} \sim \lambda(TR)^{1/2}$ and $\theta \sim (TR)^{-3/2}$. Hence, the correction goes like $(\lambda(TR)^2)^{m+1}$. Clearly these corrections cannot be ignored in the high temperature regime.

However, we expect that when $TR \gg 1$ then the eigenvalue distribution will satisfy $\theta_p, |\boldsymbol{x}_p| \ll 1$. With these assumptions, the high temperature action is found to be

$$S_{TR\gg1} = \frac{N\pi^2 TR}{\lambda} \sum_{p=1}^{N} |\boldsymbol{x}_p|^2 - \frac{1}{2} \sum_{pq=1}^{N} \log\left(|\boldsymbol{x}_{pq}|^2 + \theta_{pq}^2\right) + \pi^2 R^3 T^3 \sum_{pq=1}^{N} \left(|\boldsymbol{x}_{pq}|^2 + 2\theta_{pq}^2\right) . \tag{6.2}$$

The validity of the assumptions is verified a posteriori from the solution. The large N equations of motion following from this action may be written

$$P\boldsymbol{x} = \int d^6x' \, d\theta' \, \rho(\boldsymbol{x}', \theta') \frac{(\boldsymbol{x} - \boldsymbol{x}')}{|\boldsymbol{x} - \boldsymbol{x}'|^2 + (\theta - \theta')^2} ,$$

$$Q\theta = \int d^6x' \, d\theta' \, \rho(\boldsymbol{x}', \theta') \frac{\theta - \theta'}{|\boldsymbol{x} - \boldsymbol{x}'|^2 + (\theta - \theta')^2} , \tag{6.3}$$

where $P = \pi^2 TR(1/\lambda + 2R^2T^2)$ and $Q = 4\pi^2 R^3 T^3$. These equations have more than one interesting solution. Once again, by application of the seven dimensional operator $\boldsymbol{\nabla}^2(\boldsymbol{\nabla}\cdot)$ in the $(\boldsymbol{x}, \theta)$ space, we can argue that non-trivial solutions to the equations of motion must be hypersurfaces in seven dimensions. For a given P and Q there are two solutions which preserve the $SO(6)_R$ symmetry. One is topologically $\boldsymbol{S}^6$ and the other is topologically $\boldsymbol{S}^5$. We expect one of these maximally symmetric solutions to have the lowest action. Before discussing the solutions, we comment on a scaling property of the solutions with P and Q. In appendix C we present various solutions that do not preserve the full R symmetry.

6.1 Scaling of the solutions and action

The effect of changing the coupling or the temperature of the theory is incorporated in the values of P and Q in the high temperature equations of motion (6.3). Under the rescaling

$$\tilde{P} = \mu P, \qquad \tilde{Q} = \mu Q, \tag{6.4}$$

the equations of motion and the normalisation condition (3.5) imply that the solution remains the same and scales to

$$\tilde{\boldsymbol{x}} = \frac{1}{\sqrt{\mu}} \boldsymbol{x}, \qquad \tilde{\theta} = \frac{1}{\sqrt{\mu}} \theta . \tag{6.5}$$

The action evaluated on the scaled solution becomes

$$S[\tilde{\boldsymbol{x}}, \tilde{\theta}] = S[\boldsymbol{x}, \theta] + \frac{1}{2} \log \mu \,. \tag{6.6}$$

We can use this scaling property to fix Q and work with P/Q. When we do numerics shortly, it will be convenient to work with $Q = 1$. Even though this value is not in the high temperature regime, we simply have to scale the solutions as we have just described. Note that

$$\frac{P}{Q} = \frac{1}{4} \frac{1}{(TR)^2 \lambda} + \frac{1}{2} \,, \tag{6.7}$$

so that $P/Q \to \infty$ corresponds to $(TR)^2 \lambda \ll 1$, whereas $P/Q \to 1/2$ corresponds to high temperatures $(TR)^2 \lambda \gg 1$ with the caveat $(TR)\lambda \ll 1$. The solution in this regime only depends on the combination $(TR)^2 \lambda$ and so, increasing or decreasing this parameter can also be interpreted as varying the value of the 't Hooft coupling λ, at a fixed temperature and at weak coupling.

6.2 S^5 solutions

These have $\theta = 0$ and preserve the full R symmetry group of the theory in the large N limit. We can write the eigenvalue density

$$\rho(\boldsymbol{x}, \theta) = \frac{\delta(\theta)\delta(|\boldsymbol{x}| - r)}{\pi^3 r^5} \,, \tag{6.8}$$

where the radius is

$$r = \frac{1}{\sqrt{2P}} \,. \tag{6.9}$$

Evaluating the action on the solution gives

$$\frac{1}{N^2} S_{\boldsymbol{S}^5} = \frac{5}{24} + \frac{1}{2} \log 2P \,. \tag{6.10}$$

These solutions are fully collapsed in the θ direction, $\rho(\theta) = \delta(\theta)$. At low temperatures, these are unstable saddle point configurations, but play an important role at high temperatures as we show below.

6.3 Ellipsoidal S^6 solutions

We now find the solutions which preserve $\mathrm{SO}(6)_R$ symmetry and where the eigenvalues spread out into a (closed) six dimensional surface in $\mathbb{R}^7$. These are the high temperature continuations of the ellipsoids we found at intermediate temperatures.

We can parametrise the surface by

$$\theta = f(r) \,, \tag{6.11}$$

where as before (although now without the factor or λ) $r = |\boldsymbol{x}|$. The induced metric on this surface is

$$ds^2 = (1 + f'(r)^2)dr^2 + r^2(d\phi^2 + \sin^2 \phi \, d\Omega_4^2). \tag{6.12}$$

Thus, for instance, for a sphere of radius A we have $f(r) = \pm\sqrt{A^2 - r^2}$ while for an ellipsoid with semi-axes A and B, $f(r) = \pm B\sqrt{1 - r^2/A^2}$. Note that the parametrisation we are using forces us to consider the solution in terms of two separate components. We now proceed to derive an action whose variation determines $f(r)$.

By SO(6) symmetry, the most general spectral density for the eigenvalue distribution at large N must be of the form

$$\rho(\boldsymbol{x}, \theta) = g(r)\ (\delta(\theta - f(r)) + \delta(\theta + f(r))) \tag{6.13}$$

where $f(r)$ is taken to be positive. We can now determine the action restricted to the SO(6) symmetric ansatz. As we will be reducing the problem to one dimension, it is convenient to introduce the effective spectral density

$$G(r) = 2\pi^3 r^5 \sqrt{1 + f'(r)^2}\, g(r)\,. \tag{6.14}$$

The high temperature action is therefore rewritten as

$$\frac{1}{N^2}S = \int dr\, G(r)(Pr^2 + Qf(r)^2) - \frac{2}{3\pi} \int dr \int dr' \int_0^\pi d\phi \sin^4\phi \tag{6.15}$$
$$\times G(r)\, G(r') \log\left(|\mathbf{r} - \mathbf{r}'|^2 + (f(r) - f(r'))^2\right)\left(|\mathbf{r} - \mathbf{r}'|^2 + (f(r) + f(r'))^2\right)\,.$$

We should also add a Lagrange multiplier term that implements the normalisation constraint: $\mu\left(\int dr G(r) - 1\right)$. By functionally differentiating with respect to G and f we can show that this action consistently leads to the equations of motion restricted to our SO(6) ansatz.

It is possible to perform the ϕ integral in (6.15) using contour integration. The answer is

$$\frac{1}{N^2}S = \int dr\, G(r)(Pr^2 + Qf(r)^2) - \frac{1}{2}\int dr \int dr'\, G(r)\, G(r')\left[\log rr' + \frac{7}{12} - \log 2\right.$$
$$\left. + \log\left(\sqrt{K^2 + 1} + \sqrt{K^2 - 1}\right) - \frac{2}{3}\frac{3K^2\sqrt{K^4 - 1} + 4(K^4 - 1)}{(\sqrt{K^2 + 1} + \sqrt{K^2 - 1})^4} + f(r') \to -f(r')\right]$$
$$+ \mu\left(\int dr G(r) - 1\right), \tag{6.16}$$

where

$$K^2 = \frac{r^2 + r'^2 + (f(r) - f(r'))^2}{2rr'}\,. \tag{6.17}$$

In (6.16) we have reduced the problem to one dimension. Variation of this action leads to a pair of integral equations for $f(r)$ and $G(r)$. We have solved these equations numerically using a simple Monte Carlo algorithm. The algorithm discretises the r axis into N points: $\int dr G(r) \to \sum_{i=1}^N$ and then minimises the multiparticle action (6.16) by relaxation. A test of our code is that at the point with enhanced SO(7) symmetry, when $P = Q$, it correctly reproduces a six sphere of radius $1/\sqrt{2P}$. The action of this configuration may be found analytically to be

$$\left.\frac{1}{N^2}S_{\boldsymbol{S}^6}\right|_{P=Q} = \frac{107}{120} + \frac{1}{2}\log\frac{P}{2}\,. \tag{6.18}$$
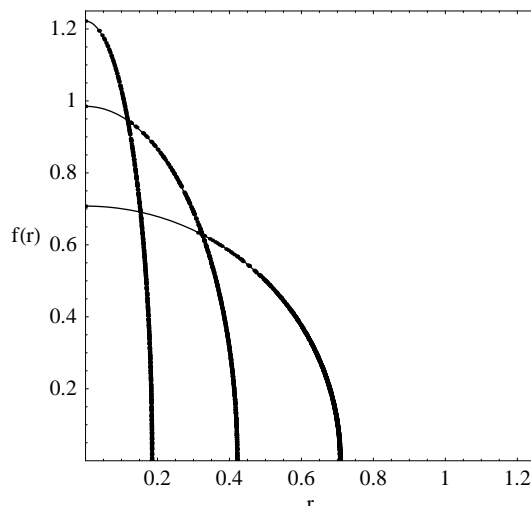
Figure 2: Output from the Monte Carlo simulation for $\{P, Q\} = \{5, 1\}, \{2, 1\}, \{1, 1\}$ with $N = 500, 500, 1000$ points, respectively. The solid lines are ellipses with axis ratio determined by the data.

The numerically obtained action agrees with this exact result to three significant figures, even with a fairly small number of points, $N \sim 60$ or so. Our main interest is for $P \neq Q$, for which we currently do not have analytic results.

The equations that we are solving numerically are very similar to those considered in the recent paper [5], which was in a supersymmetric context. The two main differences are firstly that we are looking for the semiclassical, $N \to \infty$, saddle point, whereas [5] perform a quantum Monte Carlo simulation to study the finite N wavefunction. Secondly, we have restricted to an SO(6) invariant ansatz before applying numerics. This gives a more efficient use of eigenvalues, which are diluted in fewer dimensions. However, it means that the SO(6) symmetry is a (consistent) input assumption. The numerics in [5] did not assume this symmetry but found it in their results. This provides the complementary information that the SO(6) ansatz is stable against R symmetry breaking perturbations.

Figure 2 shows the eigenvalue distributions obtained for three values of P/Q. The form is roughly what we could have anticipated, given that as P is increased the external force pushing the eigenvalues to small r becomes greater. The eigenvalue distributions appear to be ellipsoids to a very high degree of accuracy. This is perhaps not surprising given our results from the intermediate temperature regime. The numerics are not accurate enough to reliably read off a density profile.

The gap in the data points at small r in figure 2 is due to the fact that the effective density, $G(r)$, is very low in this region. This is due to the r^5 term in (6.14). Note however that there is a data point at $r = 0$ for all three curves. The solid lines in figure 2 are the ellipses determined by the extent of the distribution in the r and f directions. These curves match all the numerically obtained data points to two significant figures.

Given the appearance of ellipsoids, a rescaling-invariant question we can ask is how
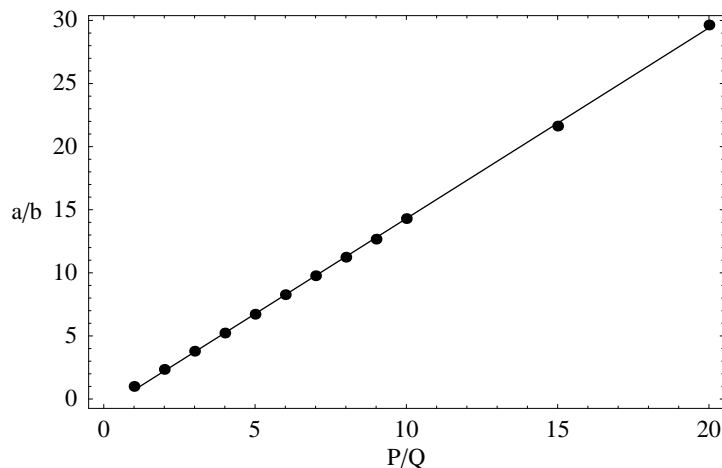
Figure 3: The axis ratio of the ellipsoidal distribution as a function of P/Q, with $Q = 1$. The data points are from the Monte Carlo numerics whereas the solid line is a linear fit.

the axis ratio of the ellipsoid varies with P/Q. Figure 3 is a plot showing the axis ratio at several values of P/Q. There appears to be a linear relation between these quantities to good approximation over the range plotted. Figure 3 also shows a linear fit to the data points for $P/Q \geq 2$. The best fit line is

$$\frac{a}{b} = -0.81 + 1.51\frac{P}{Q}, \tag{6.19}$$

where a and b are the lengths of the axis in the f and r directions, respectively.

In the limit where $\lambda(TR)^2 \ll 1$, or P/Q large, we can compare the axis ratio with that of the ellipsoid we found in the intermediate temperature regime (5.11). In terms of P/Q it follows from (5.11) that the axis ratio for those ellipsoids is also linear in P/Q

$$\frac{a}{b} = \frac{945\pi}{2048}\frac{P}{Q} \approx 1.45\frac{P}{Q}. \tag{6.20}$$

This is fairly close to (6.19), especially given that the fit (6.19) included a range of points outside the region of validity of (5.11). A more precise matching comes from taking, for instance, the value $P/Q = 20$. This corresponds to $\lambda(TR)^2 \sim 1/80$, and so should be well described by the intermediate temperature analysis. For this value we find that the numerical axis ratio is 29.6 whereas the analytic result is 29.0. This close agreement is a test of both the numerics and analytic results.

Finally, we can compute the action of the solution as a function of P/Q. The result is shown in figure 4 for $Q = 1$. We have also included in the plot the action of the round $\boldsymbol{S}^5$ solution and the action of the two dimensional ellipse solution discussed in [19].

As with the axis ratio, at large P/Q we can compare the numerically obtained actions with the analytic result in the intermediate temperature regime. At $P/Q = 20$ the numerically found action is 1.04 and the action of the ellipsoid (5.11) is 1.09.
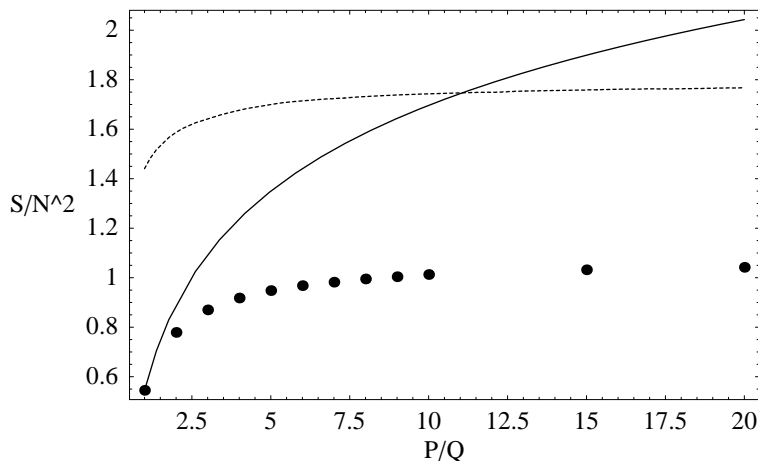
Figure 4: The action of three different eigenvalue configurations as a function of P/Q with $Q = 1$. The data points are from the $\boldsymbol{S}^6$ ellipsoid. The solid curve is the round $\boldsymbol{S}^5$ solution. The dotted curve is the two dimensional ellipse solution.

We see that throughout the range plotted, $P/Q \geq 1$, the ellipsoidal eigenvalue distribution has the lowest action and therefore dominates the partition function. Therefore, at sufficiently weak coupling, the ellipsoidal distributions describe the vacuum of the theory. However, as P/Q is lowered past 1, recall that lowering P/Q corresponds to either increasing the temperature at fixed weak coupling or increasing the (weak) coupling at fixed temperature, it looks like the curves for $\boldsymbol{S}^5$ and the six dimensional ellipsoid might cross. This raises the prospect of a new phase transition in the high temperature regime as a function of coupling.

7. A second order phase transition: $\boldsymbol{S}^6 \to \boldsymbol{S}^5$

In figure 4 we saw that as the coupling is increased at fixed high temperature, the action for the $\boldsymbol{S}^5$ solution comes closer and closer to that of the, increasingly anisotropic, ellipsoidal $\boldsymbol{S}^6$ solution. At the point with enhanced SO(7) where we have analytic results, $P = Q = 1$, the difference between the actions is surprisingly small, given that $P/Q = 1$ is not particularly close to the asymptotic regime $P/Q \to 1/2$

$$\frac{1}{N^2} \left[S_{\boldsymbol{S}^6} - S_{\boldsymbol{S}^5} \right]_{P=Q=1} \approx -0.0098 \,. \tag{7.1}$$

What happens as P/Q is decreased below this value? We now give four arguments that, taken together, strongly suggest that a second order phase transition occurs in the commuting saddle at $\lambda(TR)^2 = 1$, or $P/Q = 3/4$. This is the curve that we included in figure 1 above.

7.1 The actions converge

Figure 5 shows the action from the numerical computation together with the analytically computed action of the round $\boldsymbol{S}^5$ solution (6.10) as a function of P/Q, for $0.7 \leq P/Q \leq 1.2$.
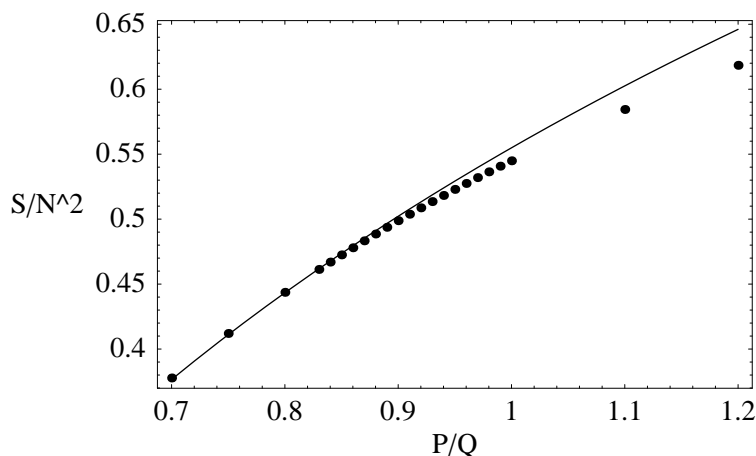
Figure 5: The data points are the numerically computed action (with $N = 150$). The curve is the action of the S^5 solution.

We see that to within the accuracy of the numerical computation, the error seems to be under 0.5%, the numerical data joins the curve of the S^5 action somewhere around $P/Q \sim 0.75$ or 0.8 and then follows this curve for lower P/Q.

The simplest interpretation of figure 5 is that beyond some critical coupling, such that $P/Q \sim 0.75$ or 0.8, the S^5 saddle becomes the lowest action configuration. The Monte Carlo simulation therefore converges on the S^5 saddle below this value. If this indeed occurs, it indicates that there is a quantum phase transition at the critical coupling in which the vacuum manifold of eigenvalues changes topology: $S^6 \to S^5$. It is a quantum phase transition in the sense that it is not associated with any symmetry breaking and the different phases have topological characterisations. It is possible however to write down non-topological "order parameters" that go from non-zero to zero as we cross the transition, such as $\langle \boldsymbol{x}^2 \rangle^2 - \langle \boldsymbol{x}^4 \rangle$. It should be clear from this order parameter that the transition will not be visible if the scalars are integrated out.

The convergence of actions does not tell us whether the possible transition is first or second order. We will now show analytically that at $P/Q = 0.75$ the S^6 saddle becomes completely localized in the θ direction and becomes a round S^5. Furthermore, we we will find zero modes about the S^5 solution at precisely $P/Q = \frac{3}{4}$ which provide compelling evidence that there is indeed a second order phase transition.

7.2 The S^6 collapses to S^5

Motivated by the numerical results above, we now look for an analytical condition on the parameters P and Q, for the S^6 solution to collapse to an S^5. The central fact we will use is the existence of the S^6 saddle for an appropriate parameter range, a fact which we have established both numerically and analytically for a wide range of temperatures. In the temperature range $TR \gg 1$, the S^6 topology solves the equations (6.3).

Since the S^6 solution is actually a round S^5 fibred over a finite interval in the θ

direction, we may differentiate the second equation of motion (6.3) with respect to θ to obtain a condition which must be fulfilled by the same solution:[4]

$$Q = \int d^6x' \, d\theta' \, \rho(\boldsymbol{x}',\theta') \frac{|\boldsymbol{x}-\boldsymbol{x}'|^2 - (\theta-\theta')^2}{(|\boldsymbol{x}-\boldsymbol{x}'|^2 + (\theta-\theta')^2)^2} \,. \tag{7.2}$$

We emphasize that this will be automatically satisfied by the SO(6) symmetric $\boldsymbol{S}^6$ topology, since the equation of motion holds at each point on the support of $\rho(\boldsymbol{x},\theta)$ in the θ direction.

We now want to find at what temperature the extent of the effective distribution in θ shrinks to zero size, and thus the $\boldsymbol{S}^6$ collapses to an $\boldsymbol{S}^5$. In such a limit, we expect the density function $\rho(\boldsymbol{x},\theta)$ to smoothly approach (6.8) with the $\boldsymbol{S}^5$ radius equal to $1/\sqrt{2P}$. Substituting these into (7.2), we find

$$\frac{Q}{P} = \frac{4}{3}. \tag{7.3}$$

It is easy to check that the integral in (7.2) is well behaved in the limit that θ, θ' approach zero, and that the limiting value of $\frac{4}{3}$ is approached from below. Hence the $\boldsymbol{S}^6$ topology ceases to exist for $Q/P > \frac{4}{3}$ which translates to $TR > \lambda^{-1/2}$, and at these temperatures with a fixed weak coupling, the equations of motion are only solved by the $\boldsymbol{S}^5$ configuration of eigenvalues.

We remark that this transition from $\boldsymbol{S}^6$ to $\boldsymbol{S}^5$ cannot be seen in the $\lambda = 0$ theory, since the critical temperature is $T = 1/(\sqrt{\lambda}R)$, and is driven by the presence of the scalar expectation values in the $\mathcal{N} = 4$ theory.

7.3 The $\boldsymbol{S}^5$ saddle develops a zero mode

Now consider the stability of the $\boldsymbol{S}^5$ solution (6.9). As mentioned above, we expect the $\boldsymbol{S}^5$ solution will be stable against perturbations in the $\boldsymbol{x}_p$ directions that would break R symmetry. It is important to check this and we do so in appendix B. However, something interesting occurs if we consider perturbations in θ_p.

Returning for the moment to the discrete system, the quadratic action for fluctuations $\delta\theta_p$ is given by

$$\delta^{(2)}S = QN \sum_{p=1}^{N} \delta\theta_p^2 - \frac{1}{2}\sum_{pq=1}^{N} \frac{(\delta\theta_p - \delta\theta_q)^2}{|\boldsymbol{x}_{pq}|^2} \,. \tag{7.4}$$

It is straightforwardly shown that in the large N limit, the N eigenvalues are all equal to $N(Q - \frac{4}{3}P)$. Hence, the solution is only stable when $Q/P > \frac{4}{3}$, that is

$$TR > \frac{1}{\sqrt{\lambda}} \,. \tag{7.5}$$

When $Q/P < \frac{4}{3}$ it is unstable to spreading out in the θ direction. We have already found the high temperature configuration with θ spread out: it is the $\boldsymbol{S}^6$ ellipsoid.

---

[4]We may do this consistently for every value of θ lying inside the distribution, and by continuity we can aslo apply the condition to all points approaching the edges of the distribution in θ-space.
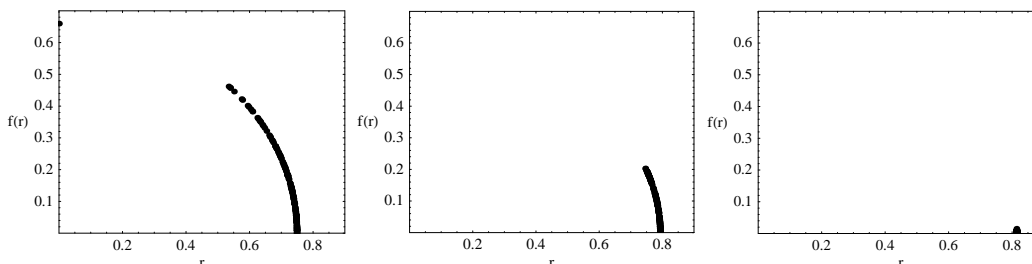
Figure 6: From left to right, the eigenvalue distributions with $P/Q = 0.9, 0.8$ and 0.75. Numerically computed with $N = 150$ eigenvalues and $Q = 1$.

The appearance of zero modes in the $\boldsymbol{S}^5$ vacuum and negative modes for $TR < \lambda^{-1/2}$, in conjunction with our earlier observation that the $\boldsymbol{S}^6$ solution merges with the $\boldsymbol{S}^5$ at $TR = \lambda^{-1/2}$, provides clear and solid evidence for a second order phase transition at this temperature.

We remark that although there are N zero modes at the transition there is only one $\boldsymbol{S}^6$ vacuum due to the action of the Weyl group permutations on the joint eigenvalues (ϕ_p, θ_p).

7.4 The eigenvalue distributions converge

In further support of this picture, let us look in more detail at the output of the numerics as $P/Q \to \frac{3}{4}$. The output no longer resembles the ellipses shown in figure 1 but rather gives a cluster of points around a radius that is very close to the radius of the $\boldsymbol{S}^5$, $1/\sqrt{2P}$ as found in (6.9) above, and $f = 0$. This is what we would expect to see if the density of eigenvalues of the $\boldsymbol{S}^6$ were accumulating on the equator as the ellipsoid becomes increasingly squashed. In the limit of this process, the solution becomes an $\boldsymbol{S}^5$.

The three graphs in figure 6 illustrate this process. As $P/Q \to \frac{3}{4}$, the eigenvalues start to cluster around $0.81 \approx 1/\sqrt{2 \times 0.75}$. As in the previous section, the gaps in the distribution are partly due to a low effective eigenvalue density (6.14) as $r \to 0$. However, we clearly see the gap growing as the eigenvalues become more densely clustered around the equator of the squashed ellipsoid.

8. Dual spacetime interpretation

A striking recent development in the supersymmetric sector of the zero temperature AdS/CFT correspondence is that the scalar field eigenvalue distribution can be directly connected to the dual spacetime geometry [2–5]. The most immediate manifestation of this connection is that the $\boldsymbol{S}^5$ part of the eigenvalue distribution is to be identified with the $\boldsymbol{S}^5$ part of the dual $\boldsymbol{AdS}_5 \times \boldsymbol{S}^5$ geometry [4]. One can think of the eigenvalue distribution as signalling the fact that the spacetime geometry has undergone a geometric transition, in which a noncontractible $\boldsymbol{S}^5$ appears, due to the gravitational backreaction of the N D3 branes. More generally, the eigenvalue distribution is to be identified with the locus in the dual spacetime where the $\boldsymbol{S}^3$ of the conformal boundary geometry degenerates [4, 5]. In $\boldsymbol{AdS}_5$ this is simply the origin of the AdS space.

The question is then whether, in our finite temperature, non supersymmetric and weak coupling setup, we can reinterpret the various topology changes undergone by our eigenvalue distributions as topology changes in a dual spacetime, analogous to the Hawking-Page transition. Although our saddles are not generically the dominant saddles, the assumption of commuting matrices does mean that they are the most 'geometric' saddles at weak coupling. At low temperatures, our $S^1 \times S^5$ distribution looks promising. This is indeed the topology of Euclidean thermal AdS at the origin of the AdS space.

The S^1 appearing in the low temperature $S^1 \times S^5$ eigenvalue distribution should in fact be associated with the T-dual of the thermal circle in spacetime, insofar as T-dualising along a thermal circle is well defined. This is because eigenvalues of the Wilson line around a circle, in our case the Polyakov-Wilson loop around the thermal circle, yield the locations of D branes in the T-dual transverse circle. Supporting this observation, the radius of the S^1 circle is proportional to the temperature T, if we renormalize the low temperature S^5 radius (3.8) to unity.

The S^6 eigenvalue distribution appearing above the first order Hagedorn transition has a natural explanation if one takes the notion of T-duality along the thermal circle seriously. In this picture, the Polyakov loop eigenvalues represent positions of D2 branes, T-dual to the original D3 branes, along the T-dual circle. The gapped distribution of the Polyakov loop eigenvalues above the Hagedorn transition is then a localized distribution of D2 branes on this circle. A similar localization of D2 branes on a *spatial* circle, at finite temperature, has been argued [20] to produce a near horizon geometry containing a non-contactible S^6. In that case, somewhat tantalizingly, an $S^1 \times S^5 \to S^6$ topological transition of the Gregory-Laflamme type was predicted from supergravity, and the localized D2 brane configuration was reinterpreted as winding mode condensation on the original circle. The interpretation of a nonuniform eigenvalue distribution as smeared branes has also been used previously to good effect in studying a field theory dual of the Gragory-Laflamme black string instability in [21].

From the weakly coupled field theory perspective, the connection to a D2 brane setup above the Hagedorn/deconfinement temperature and below $T = 1/(\sqrt{\lambda}R)$, perhaps suggests that the field theory is in an effectively three dimensional phase in that region of the phase diagram. The potential appearance of an S^6 topology in the dual spacetime would be consistent with this line of thinking: At any fixed temperature, as the 't Hooft coupling is decreased so that string corrections become substantial, at a critical coupling, when the size of the thermal circle in string units becomes sufficiently small, the theory undergoes a stringy transition resulting in the S^6 topology.

More interesting is the possible dual spacetime interpretation of the S^5 topology above the second order transition at $TR = \lambda^{-1/2}$. It is tempting to identify this topology as the deep interior of the big black hole in $AdS_5 \times S^5$ wherein the thermal circle has shrunk to zero size at the horizon. The simplest phase diagram implied by the new phase transition, shown in figure 1, also suggests that this phase might be the continuation to weak coupling of the big black hole in AdS space.

It is natural to try to associate the disappearance of the product S^1 factor in the eigenvalue distribution with the appearance of a black hole in the dual geometry. However,

it is difficult to make this connection precise. For a start, in black hole geometries the spatial S^3 never collapses. The Euclidean thermal circle degenerates at the horizon instead. The zero temperature connection of the eigenvalue distribution to the locus of vanishing S^3s in the dual spacetime will need to be modified in the non-supersymmetric thermal situation for a spacetime interpretation of the eigenvalue distributions to be possible. Since these distributions characterize the ground state or the deep IR of the thermal field theory on S^3, it is possible that they provide information about the deep interior of the dual geometry.

9. Discussion and conclusions

In this paper we have studied weakly coupled finite temperature $\mathcal{N} = 4$ super Yang-Mills theory on a spatial S^3, in the large N limit. The main difference between our work and previous treatments, [7] being the most important, is that we have considered the effects of condensed eigenvalues for the six scalar fields of the theory, as well as the time component of the gauge field, A_0. These scalar eigenvalues have been studied recently in the zero temperature theory [4, 5] where their condensate is directly related to the dual spacetime geometry. The scalar eigenvalues condense despite having conformal and thermal masses because there is a logarithmic repulsion between the eigenvalues, which at large N overcomes the mass squared terms.

We have only studied certain special saddle points of the full large N theory, in which the homogeneous modes of the fields $\{A_0, \Phi_J\}$ condense and commute with each other. Although these are not generically the dominant saddles, and thus do not determine the phase structure of the theory, they have several interesting features. Firstly, they are tractable saddles that preserve the full $\mathrm{SO}(6)_R$ symmetry of the theory. We have seen that they undergo nontrivial dynamics as a function of temperature and coupling. More speculatively, because these are the most geometric saddles at weak coupling, one can wonder whether they have any connection with the geometry that arises in the strongly coupled theory via the AdS/CFT duality. For instance, if a mechanism similar to that described in [4] is responsible for the emergence of spacetime geometry at finite temperature, then the strongly coupled theory will be described by a commuting saddle point. In this scenario, our weak coupling saddles would be continuously connected to the strong coupling supergravity geometry.

At low temperatures and through the Hagedorn phase transition into the deconfined phase, the picture of [7] is not fundamentally modified. The eigenvalue distribution of A_0 which that paper considered becomes part of a higher dimensional distribution: $S^5 \times S^1$ at low temperatures and an ellipsoidal S^6 above the transition. However, at sufficiently high temperature $TR = \lambda^{-1/2}$, or alternatively, when the coupling becomes sufficiently strong (but still small) we found evidence for a new second order phase transition, in the commuting saddle. This transition is directly due to the backreaction of the scalar field eigenvalues on the eigenvalues of A_0. Therefore, this transition could not have been seen without inclusion of the scalar field eigenvalues. In terms of distributions, at the transition: $S^6 \to S^5$.

We presented four pieces of evidence for a second order phase transition in the weakly coupled theory at $\lambda = 1/(TR)^2$, with $TR \gg 1$. Firstly, we found numerically that the actions of the $\boldsymbol{S}^5$ and $\boldsymbol{S}^6$ saddles meet at this coupling. Secondly, we showed analytically that the $\boldsymbol{S}^6$ solution collapses to $\boldsymbol{S}^5$. Thirdly, the $\boldsymbol{S}^5$ solution develops a zero mode at precisely this point. Finally, we numerically showed how the $\boldsymbol{S}^6$ distribution becomes increasingly squashed and approaches an $\boldsymbol{S}^5$ at this coupling.

An application of the results in this paper is that they will allow the computation of the Maldacena-Polyakov loop at weak coupling in the commuting saddles. This is a thermal Wilson loop involving both the gauge potential and the scalar fields, which arises naturally in the $\mathcal{N} = 4$ theory. These loops may be computed at strong coupling [23] and are therefore an interesting observable to compare at weak and strong couplings. It would be interesting to understand how the $\boldsymbol{S}^6 \to \boldsymbol{S}^5$ phase transition we have discussed is reflected in the value of these loops.

Acknowledgments

A. Stability of the solutions

In this appendix, we will consider the stability of some of our solutions. In particular, we shall consider both the high and low temperature $\boldsymbol{S}^5$ solutions. We only consider the stability to perturbations in $\boldsymbol{x}_p$ and θ_p, and not to other modes that we have integrated out.

The high temperature $\boldsymbol{S}^5$. We begin with the high temperature $\boldsymbol{S}^5$ solution of section 6.2. By choosing $\sum_p \boldsymbol{x}_p = \sum_p \theta_p = 0$, and scaling the $\boldsymbol{x}_p$ and θ_p appropriately, the discrete action (6.2) has the form

$$S = -\frac{1}{2} \sum_{pq=1}^{N} \log \left(|\boldsymbol{x}_{pq}|^2 + \theta_{pq}^2 \right) + N \sum_{p=1}^{N} \left(|\boldsymbol{x}_p|^2 + \sigma \theta_p^2 \right) \tag{A.1}$$

with $\sigma = Q/P$, The $\boldsymbol{S}^5$ solution corresponds to $\theta_p = 0$ and $|\boldsymbol{x}_p| = 1/\sqrt{2}$. Expanding around the solution to second order in the fluctuations, we have $\boldsymbol{x}_p = \frac{1}{\sqrt{2}} \boldsymbol{\Omega}_p + \delta \boldsymbol{x}_p$, where $\boldsymbol{\Omega}_p$ is a unit 6-vector, we have

$$\delta S = N \sum_{p=1}^{N} \left(|\delta \boldsymbol{x}_p|^2 + \sigma \theta_p^2 \right) - \frac{1}{2} \sum_{pq=1}^{N} \left(\frac{|\delta \boldsymbol{x}_{pq}|^2 + \theta_{pq}^2}{1 - \boldsymbol{\Omega}_p \cdot \boldsymbol{\Omega}_q} - \left(\frac{(\boldsymbol{\Omega}_p - \boldsymbol{\Omega}_q) \cdot \delta \boldsymbol{x}_{pq}}{1 - \boldsymbol{\Omega}_p \cdot \boldsymbol{\Omega}_q} \right)^2 \right) + \cdots . \tag{A.2}$$

At large N, let us estimate the orders of N of the off-diagonal relative to the diagonal terms in the quadratic form of (A.2). Firstly the off-diagonal terms. One might think that when $\delta\boldsymbol{\Omega} = \boldsymbol{\Omega}_p - \boldsymbol{\Omega}_q$ is small these can be large relative the diagonal terms. The question is: how small can $\delta\boldsymbol{\Omega}$ be for N points distributed uniformly on $\boldsymbol{S}^5$? If it were an $\boldsymbol{S}^1$ then this would be $\sim 1/N$ and so the sum over pairs in (A.2) would be of order N^2 and so the off-diagonal terms would dominate and there would be instabilities. However, on $\boldsymbol{S}^5$ the distribution of the relative angle $\cos\vartheta = \boldsymbol{\Omega}_p \cdot \boldsymbol{\Omega}_q$ is weighted by a factor $\sin^4\vartheta$. Hence, near $\vartheta = 0$ the average separation in ϑ is $\delta\vartheta$ where

$$\frac{8N}{3\pi} \int_0^{\delta\vartheta} d\vartheta \, \sin^4\vartheta = 1 \tag{A.3}$$

i.e., $\delta\vartheta \sim N^{-1/5}$. Hence, the off diagonal terms in (A.2) are at most $\mathcal{O}(N^{2/5})$ and consequently are subleading at large N and we can ignore them for the purposes of establishing stability.

To summarize, the issue of stability is determined solely by the diagonal terms; however, we shall find it necessary to go up to quartic order in order to settle the issue.

To all orders, we have

$$S + \delta S = N \sum_{p=1}^N \left(\left| \frac{1}{\sqrt{2}} \boldsymbol{\Omega}_p + \delta\boldsymbol{x}_p \right|^2 + \sigma\theta_p^2 - \sum_{q=1}^N \log\left((1 + \sqrt{2}\boldsymbol{\Omega}_p \cdot \delta\boldsymbol{x}_p)(1 - \boldsymbol{\Omega}_p \cdot \boldsymbol{\Omega}_q) + |\delta\boldsymbol{x}_p|^2 \right. \right.$$
$$\left. \left. + \theta_p^2 - \sqrt{2}\delta_\perp\boldsymbol{x}_p \cdot \boldsymbol{\Omega}_q \right) \right), \tag{A.4}$$

where $\delta_\perp\boldsymbol{x}$ are the variation perpendicular to $\boldsymbol{\Omega}_p$, i.e. tangent to $\boldsymbol{S}^5$. We can evaluate δS by replacing the sum over $\boldsymbol{\Omega}_q$ by an integral $\int d^5\boldsymbol{\Omega}$ and use

$$\sum_q \mathcal{F}(\boldsymbol{\Omega}_p \cdot \boldsymbol{\Omega}_q, \delta_\perp\boldsymbol{x}_p \cdot \boldsymbol{\Omega}_q) \longrightarrow \frac{2N}{\pi} \int_0^\pi d\psi \, \sin^3\psi \int_0^\pi \sin^4\vartheta \, \mathcal{F}(\cos\vartheta, |\delta_\perp\boldsymbol{x}_p| \sin\vartheta \cos\psi) \, . \tag{A.5}$$

This gives to quartic order,

$$\delta S = \frac{N}{3} \sum_{p=1}^N \left((3\sigma - 4)\theta_p^2 + 2(\boldsymbol{\Omega}_p \cdot \delta\boldsymbol{x}_p)^2 + 2\sqrt{2}(\boldsymbol{\Omega}_p \cdot \delta\boldsymbol{x}_p)(|\delta\boldsymbol{x}_p|^2 + 2\theta_p^2) \right. \tag{A.6}$$

$$\left. + |\boldsymbol{x}_p|^4 + 4|\delta\boldsymbol{x}_p|^2\theta_p^2 + 6\theta_p^4 \right) + \cdots \, . \tag{A.7}$$

From this, a careful analysis reveals that the solution is stable so long as $\sigma > \frac{4}{3}$ as claimed in the text. Notice that the fluctuations tangent to the $\boldsymbol{S}^5$ are only stable to quartic order.

The low temperature $\boldsymbol{S}^5$. We can prove the stability of this solution using exactly the same arguments. First of all, the action from section 3 is

$$S = \frac{\pi^2\beta R}{g^2} \sum_{p=1}^N |\phi_p|^2 - \frac{\beta}{2} \sum_{pq=1}^N |\phi_{pq}| \tag{A.8}$$

and the solution consists of an $\boldsymbol{S}^5$ with $\boldsymbol{\phi}_p = r\boldsymbol{\Omega}_p$, where we have defined the radius $r = 1024\lambda/(945\pi^3 R)$. As above only the diagonal terms play an important rôle in the large N limit. Similar methods give

$$\delta S = \frac{N\pi^2\lambda\beta}{8R}\sum_{p=1}^{N}\left((\boldsymbol{\Omega}_p \cdot \delta\boldsymbol{\phi}_p)^2 + \frac{945\pi^3}{2048}(\boldsymbol{\Omega}_p \cdot \delta\boldsymbol{\phi}_p)\big((\boldsymbol{\Omega}_p \cdot \delta\boldsymbol{\phi}_p)^2 - 6|\delta\boldsymbol{\phi}_p|^2\big)\right.$$
$$\left. - \frac{893025\pi^6}{33554432}\big(5(\boldsymbol{\Omega}_p \cdot \delta\boldsymbol{\phi}_p)^4 + 24(\boldsymbol{\Omega}_p \cdot \delta\boldsymbol{\phi}_p)|\delta\boldsymbol{\phi}_p|^2 - 24|\delta\boldsymbol{\phi}_p|^4\big)\right) + \cdots. \quad \text{(A.9)}$$

A careful analysis of this reveals expression proves that the solution is stable against all fluctuations.

B. A bestiary of saddles breaking R symmetry

As well as the absolute minima of the action discussed so far, we can also find various solutions to the effective action that do not exhibit SO(6) invariance. These solutions break the maximal R symmetry in certain patterns as we describe below. An important observation is that at any temperature they have bigger action than the dominant maximally $\mathrm{SO}(6)_R$ symmetric solutions which we have described so far. Therefore they are all unstable or metastable. These solutions may be relevant for studies of the theory at finite chemical potential.

One interesting question raised by the existence of these saddle points is whether they survive into the strong coupling regime. If they do, then presumably one should expect to find corresponding (unstable) supergravity solutions with reduced R symmetry preserved. Of the solutions that we are about to list, the lower dimensional spheres were essentially considered in [22], whereas the products and fibrations of spheres are new.

As well as the solutions described here, there are also special two dimensional 'Coulomb gas' solutions described in [19]. In those solutions only one scalar field is non-zero. That solution is also different to those listed below in that it uses the θ direction in a non-trivial way.

Low temperatures: $TR \ll 1$. Within this range of temperature, the θ distribution is uniform. Therefore there is always an $\boldsymbol{S}^1$ part of the eigenvalue distribution. In the order of increasing action, the solutions we have found are as follows:

- $\boldsymbol{S}^1 \times \boldsymbol{S}^1 \times \boldsymbol{S}^3$: The eigenvalue density is

$$\rho(\theta, \boldsymbol{x}) = \frac{\delta(|\vec{x}| - A)\delta(|\vec{y}| - \alpha A)}{8\pi^4\alpha^3 A^4}, \quad \text{(B.1)}$$

where α is the ratio of the $\boldsymbol{S}^3$ and the $\boldsymbol{S}^1$ and the vectors $\vec{x}$ and $\vec{y}$ span 2D and 4D planes respectively. The equations of motions for $\vec{x}$ and $\vec{y}$ determine the radius A and the ratio α as

$$A = \frac{\lambda C_1}{2\pi^4 TR}, \quad \text{(B.2)}$$

with $C_1 = 3.8921\ldots$ and $\alpha = 1.4344\ldots$. The action evaluated on this solution reads

$$\frac{1}{N^2} S_{\boldsymbol{S}^1 \times \boldsymbol{S}^1 \times \boldsymbol{S}^3} = -\frac{\lambda}{TR} \frac{(1+\alpha^2)C_1^2}{4\pi^6}. \tag{B.3}$$

The difference between the actions of the maximally symmetric $\boldsymbol{S}^1 \times \boldsymbol{S}^5$ solution and this $\boldsymbol{S}^1 \times \boldsymbol{S}^1 \times \boldsymbol{S}^3$ solution is then

$$\frac{TR}{\lambda} \frac{1}{N^2} \Delta S \equiv \frac{TR}{\lambda} \frac{1}{N^2} \left[S_{\boldsymbol{S}^1 \times \boldsymbol{S}^1 \times \boldsymbol{S}^3} - S_{\boldsymbol{S}^1 \times \boldsymbol{S}^5} \right] \approx 0.98 \times 10^{-5}. \tag{B.4}$$

- $\boldsymbol{S}^1 \times \boldsymbol{S}^2 \times \boldsymbol{S}^2$: The eigenvalue density is $\rho(\theta, \boldsymbol{x}) = \frac{1}{32\pi^3 A^4} \delta(|\vec{x}| - A)\delta(|\vec{y}| - A)$, where the vectors $\vec{x}$ and $\vec{y}$ span 3D planes. The radius A, action and difference in actions with the $\boldsymbol{S}^1 \times \boldsymbol{S}^5$ solution are

$$A = \frac{2\lambda(2\sqrt{2}-1)}{15\pi^2 RT},$$

$$\frac{1}{N^2} S_{\boldsymbol{S}^1 \times \boldsymbol{S}^2 \times \boldsymbol{S}^2} = -\frac{\lambda}{RT} \frac{8}{\pi^2} \left(\frac{2\sqrt{2}-1}{15}\right)^2,$$

$$\frac{TR}{\lambda} \frac{1}{N^2} \Delta S \approx 0.103 \times 10^{-4}. \tag{B.5}$$

- $\boldsymbol{S}^1 \times \boldsymbol{S}^1 \times \boldsymbol{S}^1 \times \boldsymbol{S}^1$: The eigenvalue density is $\rho(\theta, \boldsymbol{x}) = \frac{1}{16\pi^4 A^3} \delta(|\vec{x}| - A)\delta(|\vec{y}| - A)\delta(|\vec{z}| - A)$, where the vectors $\vec{x}$, $\vec{y}$ and $\vec{z}$ span 2D planes. The radius A, action and difference in actions with the $\boldsymbol{S}^1 \times \boldsymbol{S}^5$ solution are

$$A = \frac{\lambda C_2}{16\pi^5 TR} \qquad [C_2 = 98.7075\ldots],$$

$$\frac{1}{N^2} S_{\boldsymbol{S}^1 \times \boldsymbol{S}^1 \times \boldsymbol{S}^1 \times \boldsymbol{S}^1} = -\frac{\lambda}{TR} \frac{3}{256\pi^8} C_2^2.$$

$$\frac{TR}{\lambda} \frac{1}{N^2} \Delta S \approx 0.209 \times 10^{-4}. \tag{B.6}$$

- $\boldsymbol{S}^1 \times \boldsymbol{S}^4$: The eigenvalue density is $\rho(\theta, \boldsymbol{x}) = \frac{3}{16\pi^3 A^4} \delta(|\vec{x}| - A)\delta(x_6)$, where the vectors $\vec{x}$ span a 5D plane. We have

$$A = \frac{12\lambda}{35\pi^2 TR},$$

$$\frac{1}{N^2} S_{\boldsymbol{S}^1 \times \boldsymbol{S}^4} = -\frac{\lambda}{RT} \frac{12^2}{35^2 \pi^2},$$

$$\frac{RT}{\lambda} \Delta S \approx 0.144 \times 10^{-3}. \tag{B.7}$$

- $\boldsymbol{S}^1 \times \boldsymbol{S}^1 \times \boldsymbol{S}^2$: The eigenvalue density is $\rho(\theta, \boldsymbol{x}) = \frac{1}{16\pi^3 \alpha^2 A^3} \delta(|\vec{x}| - A)\delta(|\vec{y}| - \alpha A)\delta(x_6)$, where α is the ratio of the $\boldsymbol{S}^2$ and the $\boldsymbol{S}^1$ and the vectors $\vec{x}$ and $\vec{y}$ span 2D and 3D planes respectively. We have

$$A = \frac{\lambda C_3}{8\pi^3 RT} \qquad [C_3 = 5.4034\ldots],$$

$$\frac{1}{N^2} S_{\boldsymbol{S}^1 \times \boldsymbol{S}^1 \times \boldsymbol{S}^2} = -\frac{\lambda}{RT} \frac{(1+\alpha^2)C_3^2}{64\pi^4} \qquad [\alpha = 1.2404\ldots],$$

$$\frac{TR}{\lambda} \frac{1}{N^2} \Delta S \approx 0.165 \times 10^{-3}. \tag{B.8}$$

- $\boldsymbol{S}^1 \times \boldsymbol{S}^3$: The eigenvalue density is $\rho(\theta, \boldsymbol{x}) = \frac{1}{4\pi^3 A^3}\delta(|\vec{x}| - A)\delta^2(\vec{y})$, where the vectors $\vec{x}$ and $\vec{y}$ span 4D and 2D planes. We have

$$A = \frac{16\lambda}{15\pi^3 RT},$$

$$\frac{1}{N^2}S_{\boldsymbol{S}^1 \times \boldsymbol{S}^3} = -\frac{\lambda}{RT}\frac{16^2}{15^2\pi^4},$$

$$\frac{TR}{\lambda}\frac{1}{N^2}\Delta S \approx 0.374 \times 10^{-3}. \tag{B.9}$$

- $\boldsymbol{S}^1 \times \boldsymbol{S}^1 \times \boldsymbol{S}^1$: The eigenvalue density is $\rho(\theta, \boldsymbol{x}) = \frac{1}{8\pi^3 A^2}\delta(|\vec{x}| - A)\delta(|\vec{y}| - A)\delta^2(\vec{z})$, where the vectors $\vec{x}$, $\vec{y}$ and $\vec{z}$ span 2D planes. We have

$$A = \frac{\lambda C_4}{8\pi^4 RT} \quad [C_4 = 18.912\ldots],$$

$$\frac{1}{N^2}S_{\boldsymbol{S}^1 \times \boldsymbol{S}^1 \times \boldsymbol{S}^1} = -\frac{\lambda}{RT}\frac{C_4^2}{32\pi^6},$$

$$\frac{TR}{\lambda}\frac{1}{N^2}\Delta S \approx 0.428 \times 10^{-3}. \tag{B.10}$$

- $\boldsymbol{S}^1 \times \boldsymbol{S}^2$: The eigenvalue density is $\rho(\theta, \boldsymbol{x}) = \frac{1}{8\pi^2 A^2}\delta(|\vec{x}| - A)\delta^3(\vec{y})$, where the vectors $\vec{x}$ and $\vec{y}$ span 3D planes. We have

$$A = \frac{\lambda}{3\pi^2 RT},$$

$$\frac{1}{N^2}S_{\boldsymbol{S}^1 \times \boldsymbol{S}^2} = -\frac{\lambda}{TR}\frac{1}{9\pi^2},$$

$$\frac{TR}{\lambda}\frac{1}{N^2}\Delta S \approx 0.796 \times 10^{-3}. \tag{B.11}$$

- $\boldsymbol{S}^1 \times \boldsymbol{S}^1$: The eigenvalue density is $\rho(\theta, \boldsymbol{x}) = \frac{1}{4\pi^2 A}\delta(|\vec{x}| - A)\delta^4(\vec{y})$, where the vectors $\vec{x}$ and $\vec{y}$ span 2D and 4D planes. We have

$$A = \frac{\lambda}{\pi^3 R},$$

$$\frac{1}{N^2}S_{\boldsymbol{S}^1 \times \boldsymbol{S}^1} = -\frac{\lambda}{TR}\frac{1}{\pi^4},$$

$$\frac{TR}{\lambda}\frac{1}{N^2}\Delta S \approx 0.179 \times 10^{-2}. \tag{B.12}$$

Intermediate temperatures: $1 \ll TR \ll \lambda^{-1/2}$. For temperatures high enough above the deconfinement transition, we have shown above that the θ distribution is gapped. To zeroth order in λ it is given by,

$$\rho(\theta) = 4\pi(TR)^3\sqrt{\theta_0^2 - \theta^2}, \qquad \theta_0^2 = \frac{1}{2\pi^2(TR)^3}. \tag{B.13}$$

The intermediate temperature joint eigenvalue densities are obtained from the solutions listed in the previous subsection by multiplying the eigenvalue densities of the previous

subsection by $2\pi\rho(\theta)$ and letting the radii A become a function of θ, which we will denote $r(\theta)$, where

$$r(\theta) = \frac{C\lambda}{\sqrt{2}\pi RT}\rho(\theta)\,, \tag{B.14}$$

where C is now a constant that will depend on the particular solution, as we shall see below.

Combining equations (B.13) and (B.14) we find that the solutions within this range of temperature have the ellipsoidal like form:

$$\frac{\pi^2}{4C^2\lambda^2 TR}r^2 + 2\pi^2(TR)^3\theta^2 = 1\,. \tag{B.15}$$

The topology of these solutions will no longer be $\boldsymbol{S}^6$ however, but rather lower dimensional spheres and various singular spaces.

- The $\boldsymbol{S}^1 \times \boldsymbol{S}^1 \times \boldsymbol{S}^3$ solution of the previous section becomes $\boldsymbol{S}^1 \times \boldsymbol{S}^3$ fibred over an interval. Topologically, this is a singular space which may be described as an $\boldsymbol{S}^5$ in which a linked $\boldsymbol{S}^1$ and $\boldsymbol{S}^3$ have been pinched to a point. The space is described by (B.15) together with

$$x_1^2 + x_2^2 = \frac{1}{\alpha^2}(x_3^2 + \cdots + x_6^2) = r^2\,. \tag{B.16}$$

  The coefficient in (B.14) is $C = 0.557\ldots$ and as before the ratio $\alpha = 1.4344\ldots$.

- The $\boldsymbol{S}^1 \times \boldsymbol{S}^2 \times \boldsymbol{S}^2$ solution of the previous section becomes $\boldsymbol{S}^2 \times \boldsymbol{S}^2$ fibred over an interval. This is a singular space given by $\boldsymbol{S}^5$ in which two linked $\boldsymbol{S}^2$s are pinched to a point. It is described by (B.15) together with

$$x_1^2 + x_2^2 + x_3^2 = x_4^2 + x_5^2 + x_6^2 = r^2\,. \tag{B.17}$$

  The coefficient $C = \frac{4}{15}(4 - \sqrt{2})$.

- The $\boldsymbol{S}^1 \times \boldsymbol{S}^1 \times \boldsymbol{S}^1 \times \boldsymbol{S}^1$ solution of the previous section becomes $\boldsymbol{S}^1 \times \boldsymbol{S}^1 \times \boldsymbol{S}^1$ fibred over an interval. It is given by (B.15) together with

$$x_1^2 + x_2^2 = x_3^2 + x_4^2 = x_5^2 + x_6^2 = r^2\,. \tag{B.18}$$

  The coefficient $C = 0.5628\ldots$.

- The $\boldsymbol{S}^4 \times \boldsymbol{S}^1$ solution becomes a squashed $\boldsymbol{S}^5$, given by (B.15) together with

$$x_1^2 + \cdots + x_5^2 = r^2\,, x_6 = 0\,. \tag{B.19}$$

  The coefficient $C = \frac{24\sqrt{2}}{35}$.

- The $\boldsymbol{S}^1 \times \boldsymbol{S}^1 \times \boldsymbol{S}^2$ solution becomes $\boldsymbol{S}^1 \times \boldsymbol{S}^2$ fibred over an interval. Topologically this is an $\boldsymbol{S}^4$ where a linked $\boldsymbol{S}^1$ and $\boldsymbol{S}^2$ have been pinched to a point. It is given by (B.15) together with

$$x_1^2 + x_2^2 = \frac{1}{\alpha^2}(x_3^2 + x_4^2 + x_5^2) = r^2\,, x_6 = 0\,. \tag{B.20}$$

  The coefficient $C = 0.608\ldots$, and as before the ratio $\alpha = 1.2404\ldots$.

- The $\boldsymbol{S}^3 \times \boldsymbol{S}^1$ solution becomes a squashed $\boldsymbol{S}^4$, given by (B.15) together with

$$x_1^2 + \cdots + x_4^2 = r^2 \,, x_5 = x_6 = 0 \,. \tag{B.21}$$

The coefficient $C = \frac{32\sqrt{2}}{15\pi}$.

- The $\boldsymbol{S}^1 \times \boldsymbol{S}^1 \times \boldsymbol{S}^1$ solution becomes $\boldsymbol{S}^1 \times \boldsymbol{S}^1$ fibred over an interval, which is topologically and $\boldsymbol{S}^3$ with two linked $\boldsymbol{S}^1$s pinched to a point. It is given by (B.15) together with

$$x_1^2 + x_2^2 = x_3^2 + x_4^2 = r^2 \,, x_5 = x_6 = 0 \,. \tag{B.22}$$

The coefficient $C = 0.169 \ldots$.

- The $\boldsymbol{S}^1 \times \boldsymbol{S}^2$ solution goes over to a squashed $\boldsymbol{S}^3$, given by (B.15) together with

$$x_1^2 + x_2^2 + x_3^2 = r^2 \,, x_4 = x_5 = x_6 = 0 \,. \tag{B.23}$$

The coefficient $C = \frac{2\sqrt{2}}{3}$.

- The $\boldsymbol{S}^1 \times \boldsymbol{S}^1$ solution goes over to a squashed $\boldsymbol{S}^2$, given by (B.15) together with

$$x_1^2 + x_2^2 = r^2 \,, x_3 = \cdots = x_6 = 0 \,. \tag{B.24}$$

The coefficient $C = \frac{2\sqrt{2}}{\pi}$.

High Temperatures: $TR \sim \lambda^{-1/2}$. In this range of T, recall that the relevant action is

$$
\begin{aligned}
S = &\int d\theta d^6 x \rho(\theta, \boldsymbol{x}) \left(P|\boldsymbol{x}|^2 + Q\theta^2 \right) \\
&- \frac{1}{2} \int d\theta d\theta' d^6 x d^6 x' \rho(\theta, \boldsymbol{x}) \rho(\theta', \boldsymbol{x}') \log \left(|\boldsymbol{x} - \boldsymbol{x}'|^2 + (\theta - \theta')^2 \right) \,.
\end{aligned} \tag{B.25}
$$

As the temperature increases the width of the θ distribution becomes narrower. Similarly to the SO(6) symmetric case, we expect a second order phase transition to occur at a critical temperature, and for $\rho(\theta)$ to collapse to a delta function above that temperature. We will now describe R symmetry breaking solutions with

$$\rho(\theta) = \delta(\theta). \tag{B.26}$$

One finds the solutions and evaluates their actions in the same spirit as in the previous subsections. It turns out that the order of the actions evaluated on these solutions stay the same and one finds the following ordering:

$$S_{\boldsymbol{S}^1 \times \boldsymbol{S}^3} < S_{\boldsymbol{S}^2 \times \boldsymbol{S}^2} < S_{\boldsymbol{S}^1 \times \boldsymbol{S}^1 \times \boldsymbol{S}^1} < S_{\boldsymbol{S}^4} < S_{\boldsymbol{S}^1 \times \boldsymbol{S}^2} < S_{\boldsymbol{S}^3} < S_{\boldsymbol{S}^1 \times \boldsymbol{S}^1} < S_{\boldsymbol{S}^2} < S_{\boldsymbol{S}^1} \,. \tag{B.27}$$

The actions have the following values, putting $P = 1$ without loss of generality, respectively: 0.556775, 0.556853, 0.559185, 0.570093, 0.574554, 0.596574, 0.610025, 0.653427, 0.846574. We note that the first three solutions in (B.27) are extremely close to the value of the maximally symmetric solution $\boldsymbol{S}^5$ (0.554907).

– 29 –

References

[1] J.M. Maldacena, *The large-N limit of superconformal field theories and supergravity*, *Adv. Theor. Math. Phys.* **2** (1998) 231 [*Int. J. Theor. Phys.* **38** (1999) 1113] [`hep-th/9711200`].

[2] D. Berenstein, *A toy model for the AdS/CFT correspondence*, *JHEP* **07** (2004) 018 [`hep-th/0403110`].

[3] H. Lin, O. Lunin and J.M. Maldacena, *Bubbling AdS space and 1/2 BPS geometries*, *JHEP* **10** (2004) 025 [`hep-th/0409174`].

[4] D. Berenstein, *Large-N BPS states and emergent quantum gravity*, *JHEP* **01** (2006) 125 [`hep-th/0507203`].

[5] D. Berenstein and R. Cotta, *A monte-carlo study of the AdS/CFT correspondence: an exploration of quantum gravity effects*, *JHEP* **04** (2007) 071 [`hep-th/0702090`].

[6] B. Sundborg, *The Hagedorn transition, deconfinement and N = 4 SYM theory*, *Nucl. Phys.* **B 573** (2000) 349 [`hep-th/9908001`].

[7] O. Aharony, J. Marsano, S. Minwalla, K. Papadodimas and M. Van Raamsdonk, *The Hagedorn/deconfinement phase transition in weakly coupled large-N gauge theories*, *Adv. Theor. Math. Phys.* **8** (2004) 603 [`hep-th/0310285`].

[8] S.W. Hawking and D.N. Page, *Thermodynamics of black holes in Anti-de Sitter space*, *Commun. Math. Phys.* **87** (1983) 577.

[9] E. Witten, *Anti-de Sitter space, thermal phase transition and confinement in gauge theories*, *Adv. Theor. Math. Phys.* **2** (1998) 505 [`hep-th/9803131`].

[10] L. Fidkowski, V. Hubeny, M. Kleban and S. Shenker, *The black hole singularity in AdS/CFT*, *JHEP* **02** (2004) 014 [`hep-th/0306170`].

[11] G. Festuccia and H. Liu, *Excursions beyond the horizon: black hole singularities in Yang-Mills theories. I*, *JHEP* **04** (2006) 044 [`hep-th/0506202`].

[12] S.A. Hartnoll and S. Prem Kumar, *AdS black holes and thermal Yang-Mills correlators*, *JHEP* **12** (2005) 036 [`hep-th/0508092`].

[13] V.E. Hubeny, H. Liu and M. Rangamani, *Bulk-cone singularities & signatures of horizon formation in AdS/CFT*, *JHEP* **01** (2007) 009 [`hep-th/0610041`].

[14] G. Festuccia and H. Liu, *The arrow of time, black holes and quantum mixing of large-N Yang-Mills theories*, `hep-th/0611098`.

[15] P. Kovtun, D.T. Son and A.O. Starinets, *Viscosity in strongly interacting quantum field theories from black hole physics*, *Phys. Rev. Lett.* **94** (2005) 111601 [`hep-th/0405231`].

[16] H. Nastase, *The RHIC fireball as a dual black hole*, `hep-th/0501068`.

[17] O. Aharony and S.A. Hartnoll, *A phase transition in commuting gaussian multi-matrix models*, `arXiv:0706.2861`.

[18] T. Hollowood, S.P. Kumar and A. Naqvi, *Instabilities of the small black hole: a view from N = 4 SYM*, *JHEP* **01** (2007) 001 [`hep-th/0607111`].

[19] S.A. Hartnoll and S.P. Kumar, *Thermal N = 4 SYM theory as a 2D Coulomb gas*, *Phys. Rev.* **D 76** (2007) 026005 [`hep-th/0610103`].

[20] J.L.F. Barbon and E. Rabinovici, *Touring the Hagedorn ridge*, `hep-th/0407236`.

[21] O. Aharony, J. Marsano, S. Minwalla and T. Wiseman, *Black hole-black string phase transitions in thermal* $1+1$ *dimensional supersymmetric Yang-Mills theory on a circle*, Class. and Quant. Grav. **21** (2004) 5169 [`hep-th/0406210`].

[22] D. Berenstein, D.H. Correa and S.E. Vazquez, *All loop BMN state energies from matrices*, JHEP **02** (2006) 048 [`hep-th/0509015`].

[23] S.A. Hartnoll and S. Prem Kumar, *Multiply wound Polyakov loops at strong coupling*, Phys. Rev. **D 74** (2006) 026001 [`hep-th/0603190`].